Electronic Supplementary Material (ESI) for Journal of Materials Chemistry A.

Supporting Information

Layered Franckeite and Teallite Intrinsic Heterostructures: Shear Exfoliation and Electrocatalysis

*Rui Gusmão, Zdeněk Sofer, Jan Luxa and Martin Pumera**

Center for the Advanced Functional Nanorobots, Department of Inorganic Chemistry, University of Chemistry and Technology Prague, Technicka 5, 166 28 Prague 6, Czech Republic
*email: pumera.research@gmail.com

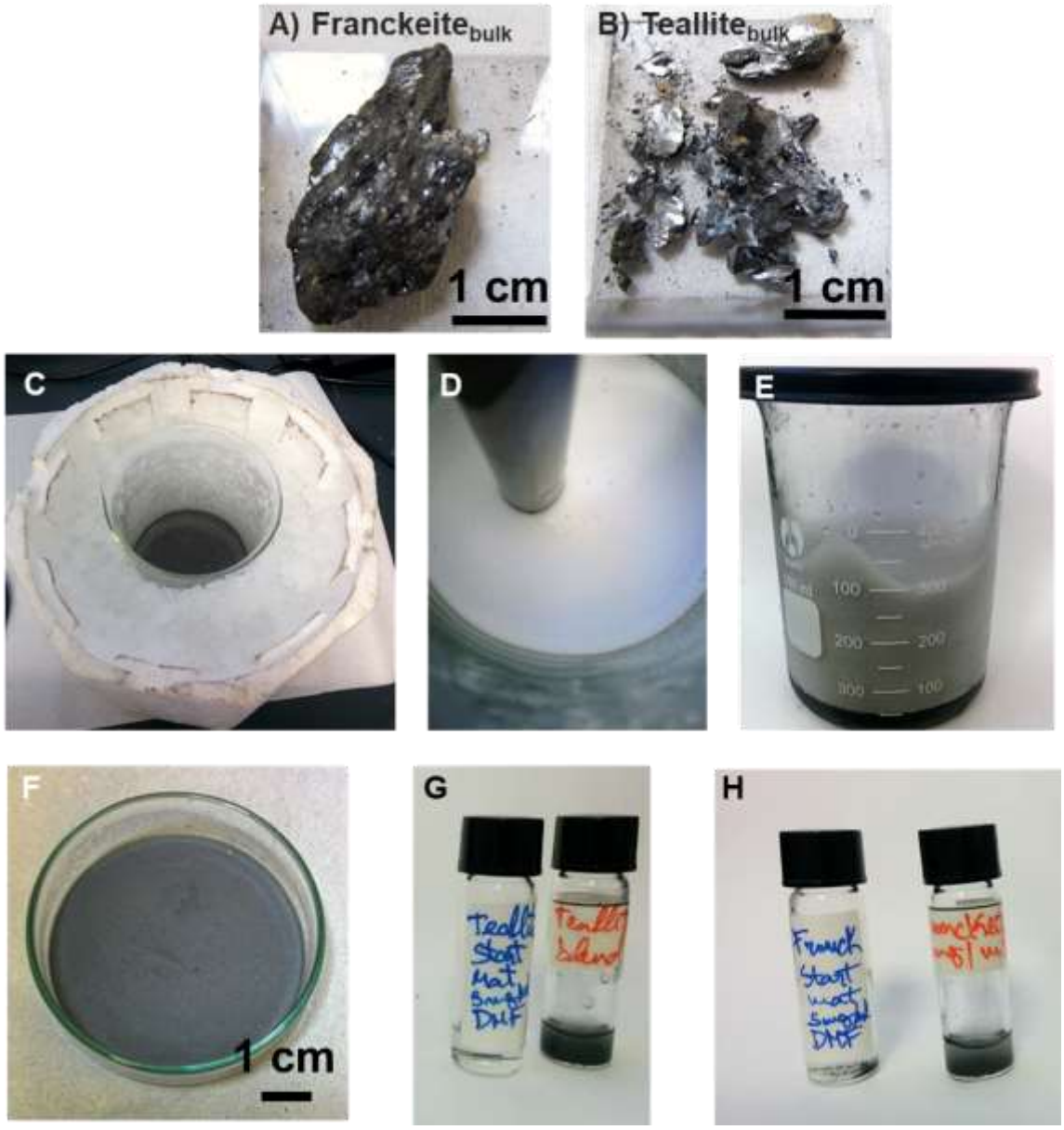

Figure S1. Photographs of the workflow for exfoliation of sulfosalts by shear force exfoliation in aqueous surfactant, sodium cholate. Initial aspect of the bulk franckeite (A) and teallite (B) crystals showing centimeter(s) size fragments. Suspension of sulfosalts in an ice bath before (C) along (D) and immediately after (E) top shear mixing using a 750 W Bosch hand blender. Right side: Photographs of final aspect of the fine powder of the shear exfoliated sulfosalts obtained from centrifugation and washing of the top 75% materials in suspension. Colloidal suspensions in DMF for teallite (G) and franckeite (H), bulk (left) and shear exfoliated (right) before sonication, showing the immediate dispersion of the exfoliated materials.

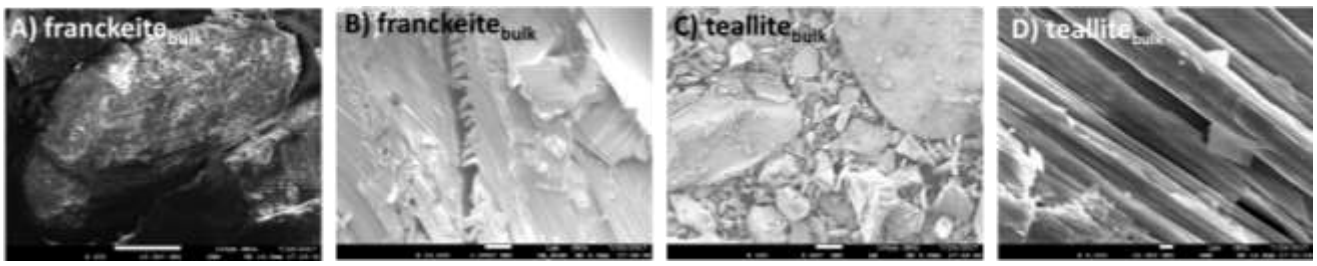

Figure S2. Sulfosalts characterization. SEM micrographs of the bulk franckeite (top A and B) and teallite (bottom C and D) crystals, scale bars represent 100 and 1 μm.

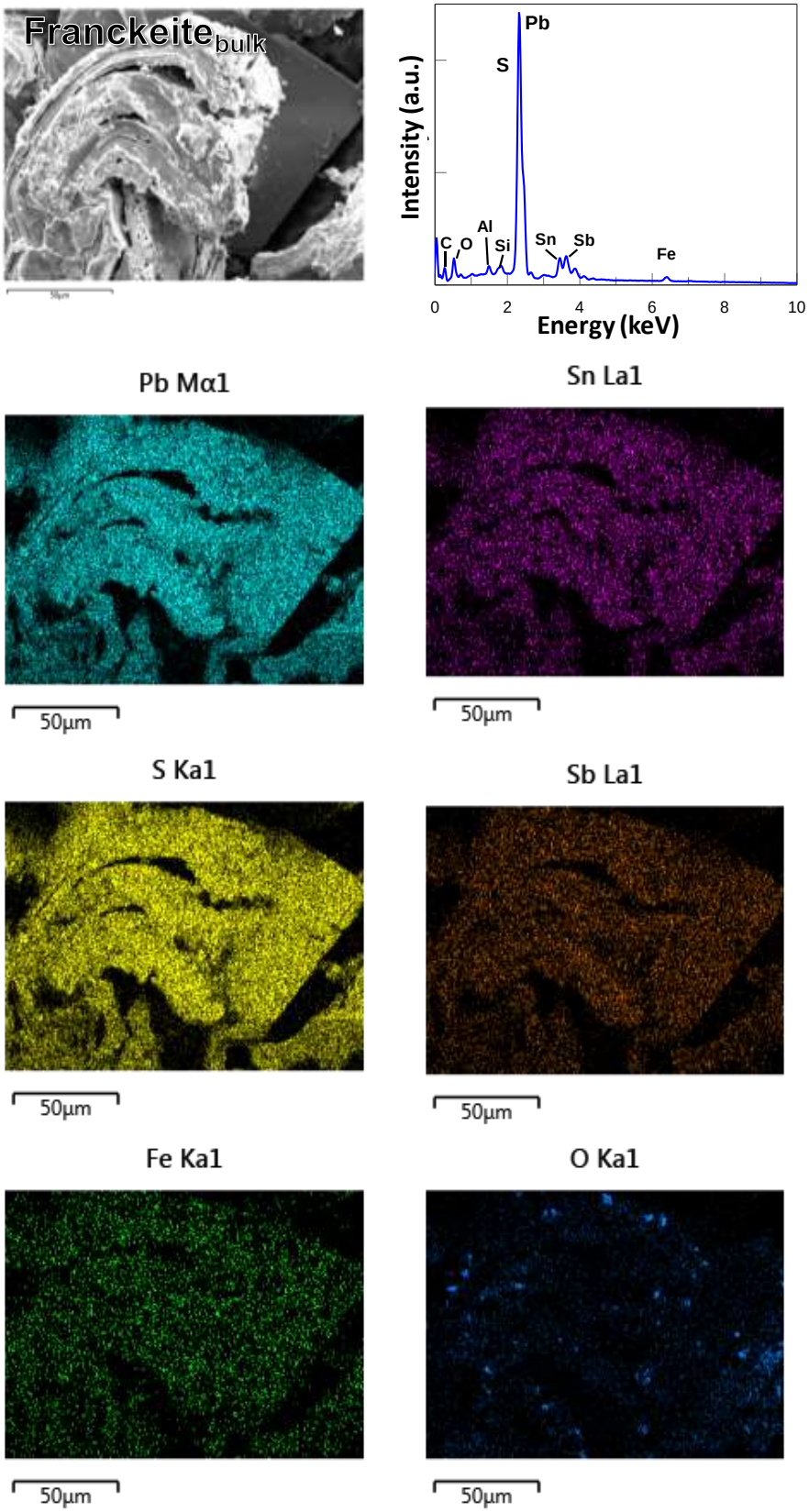

Figure S3. SEM micrograph of the bulk franckeite crystals with the respective mapping of elements, scale bars represents 50 µm. Corresponding EDX spectrum.

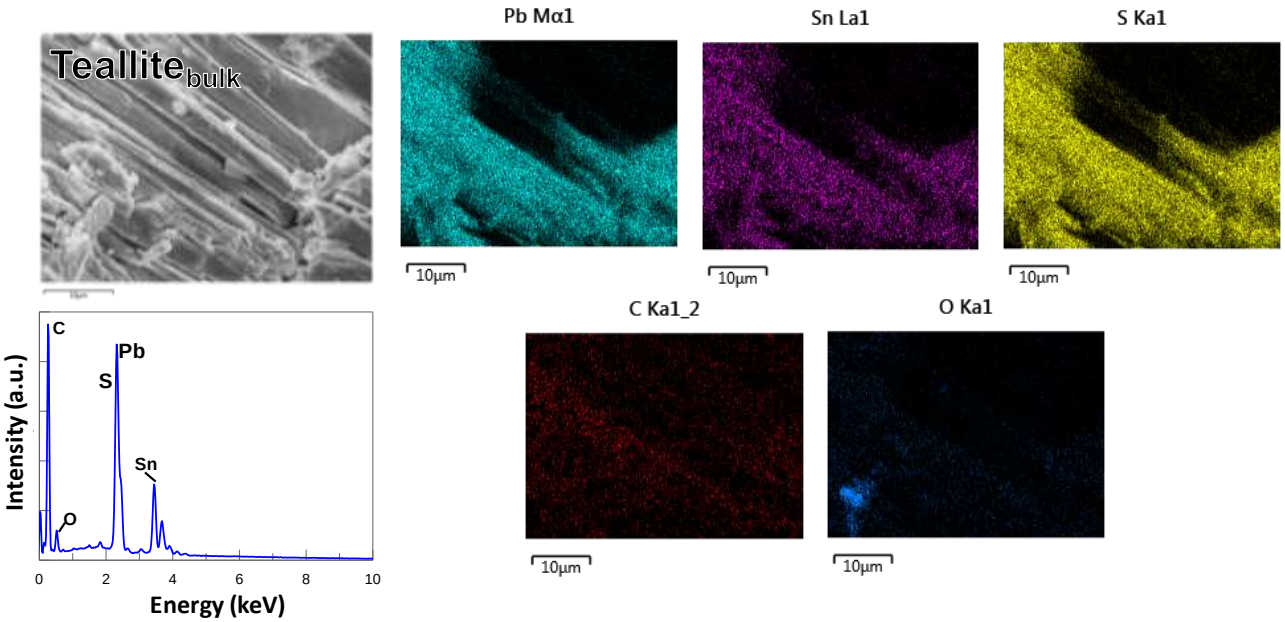

Figure S4. SEM micrograph of the bulk teallite crystals with the respective mapping of elements, scale bars represents 10 µm. Corresponding EDX spectrum.

Table S1. Average EDS quantification of elements of bulk sulfosalts (at. %) and derived empirical formula.

	Material		Derived formula	
Element	**Franckeite**	**Teallite**	**Franckeite**	**Teallite**
S	26.7 ± 2.6	33.6 ± 5.9	**12.1**	**2.9**
Pb	10.7 ± 1.1	11.6 ± 3.1	**4.9**	**1.7**
Sn	5.8 ± 1.8	19.8 ± 6.3	**2.6**	**1.0**
Sb	4.2 ± 0.8	—	**1.9**	**—**
Fe	2.2 ± 0.1	0.3 ± 0.2	**1.0**	**—**
Al	1.6 ± 0.9	0.4 ± 0.2	$Pb_{4.9}Sn_{2.6}Fe_{1.0}Sb_{1.9}S_{12.1}$	$Pb_{1.7}Sn_{1.0}S_{2.9}$
Si	0.7 ± 0.3	—		
O	11.9 ± 7.2	5.1 ± 3.5		
C	36.2 ± 13.8	29.1 ± 7.1		

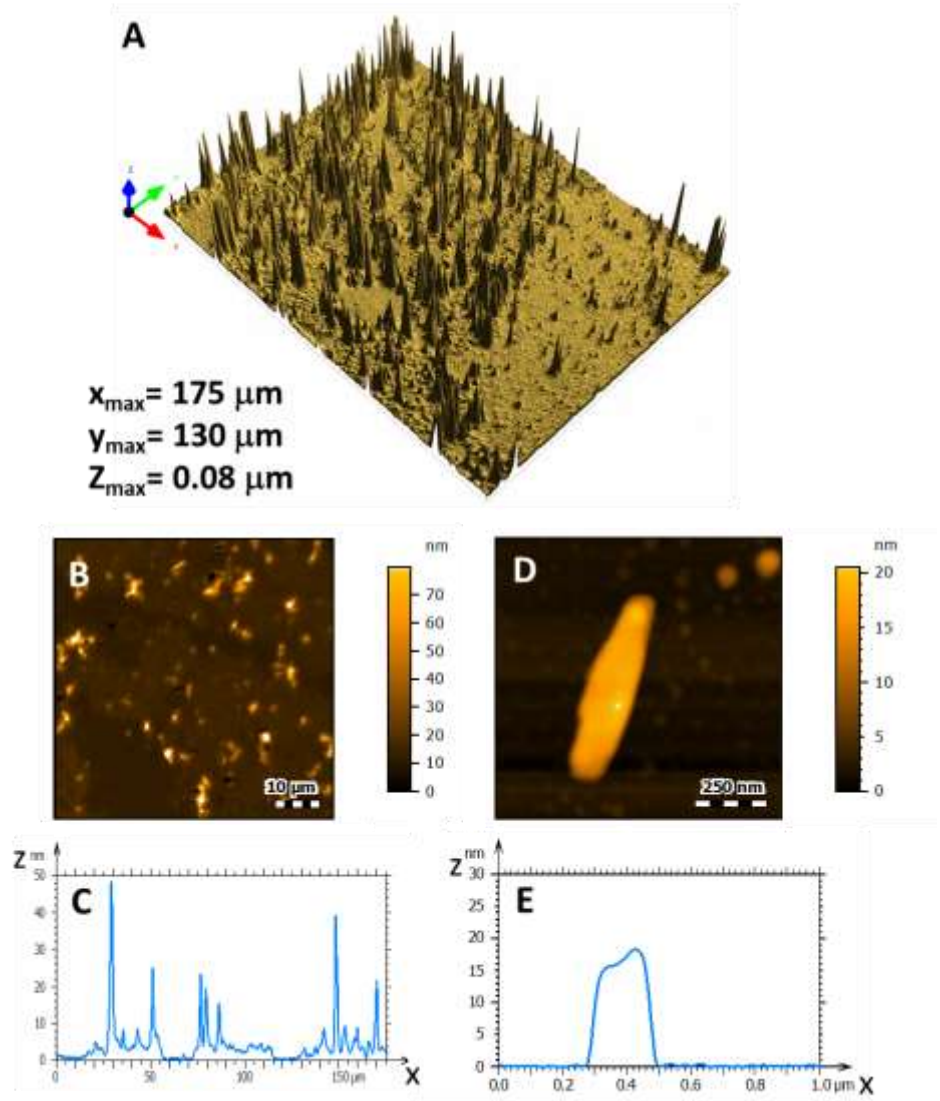

Figure S5. Franckeite$_{SE}$ nanosheets height profiles. A) 3D representation of the ITO surface observed by optical profilomenter, with dimensional block of 175x130x0.08 µm. B) Section of the surface used for height measurement. C) Example of the height profile curve distribution. D) AFM image and E) corresponding height profile.

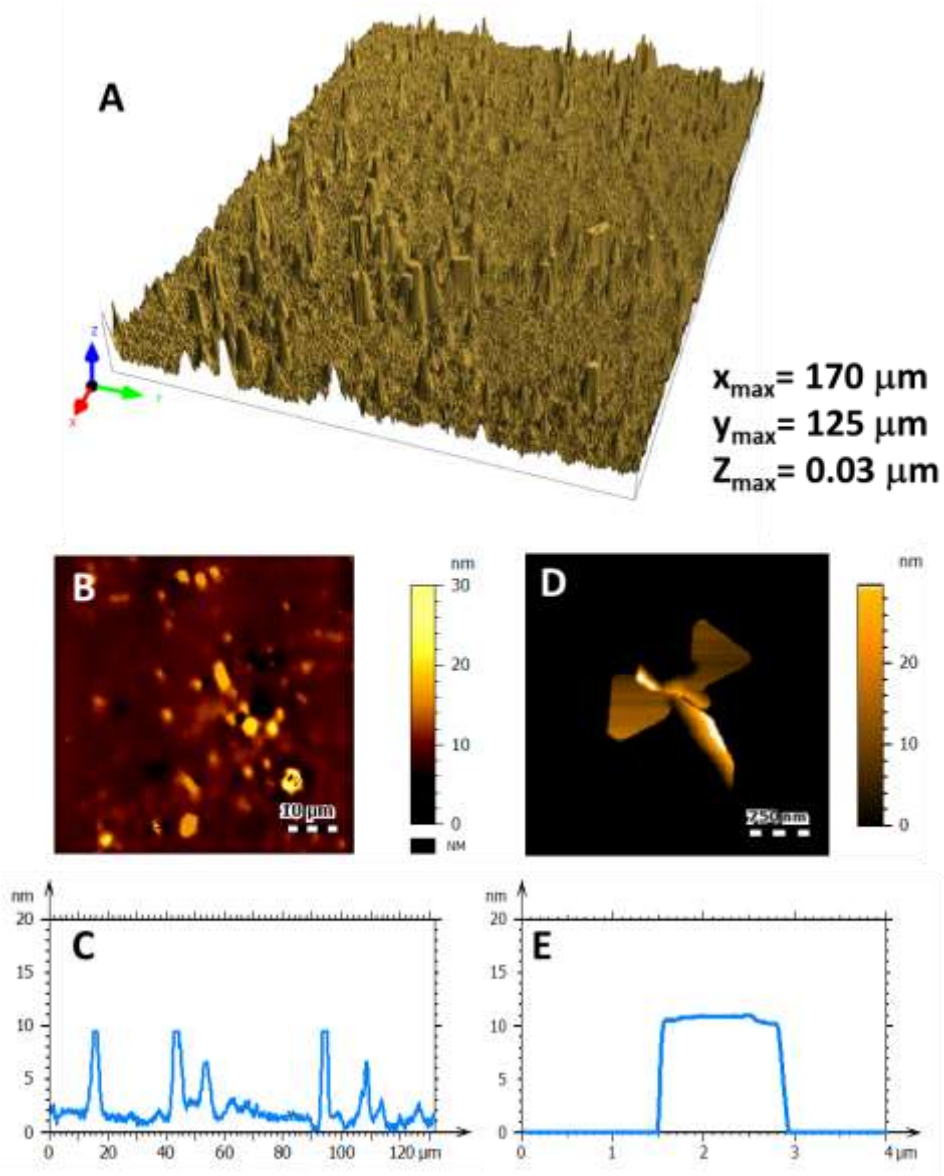

Figure S6. Teallite$_{SE}$ nanosheets height profiles. A) 3D representation of the ITO surface observed by optical profilomenter, with dimensional block of 170x125x0.03 µm. B) Section of the surface used for height measurement. C) Example of the height profile curve distribution. D) AFM image and E) corresponding height profile.

Table S2. Raman bands assignment for bulk and shear exfoliated sulfosalts.

		Raman shift / cm^{-1}			
Building block	**Phonon mode**	**Teallite $_{bulk}$**	**Tealliute$_{SE}$**	**Fracnkeite $_{bulk}$**	**Franckeite$_{SE}$**
SnS	A_g	88	88	87	84
	B_{3g}	138	140	137	139
	A_g	174	171	186	187
	A_g	213	216	204	209
Sb_2S_3				256	256
				276	277
SnS_2	A_{1g}			318	320

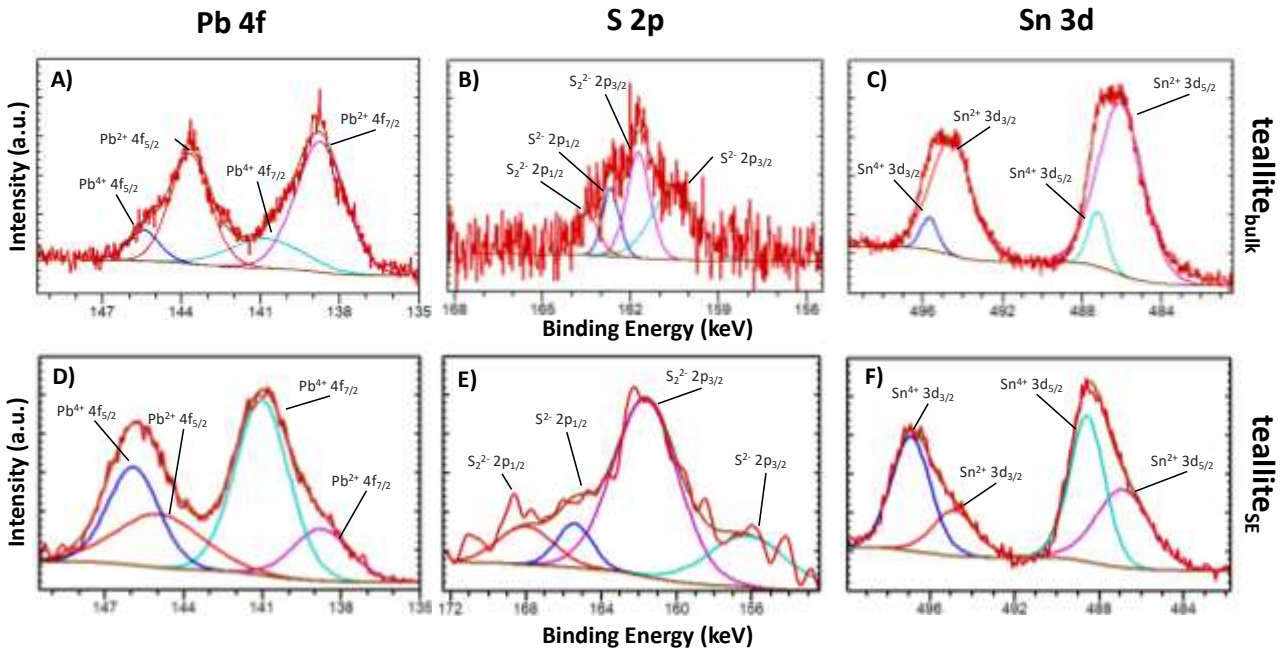

Figure S7. High-resolution spectra and deconvolution with color matching peaks components for teallite$_{bulk}$ (top row) and teallite$_{SE}$ (bottom row) of Pb 4f (A, D), S 2p (B, E) and Sn 3d (C, F).

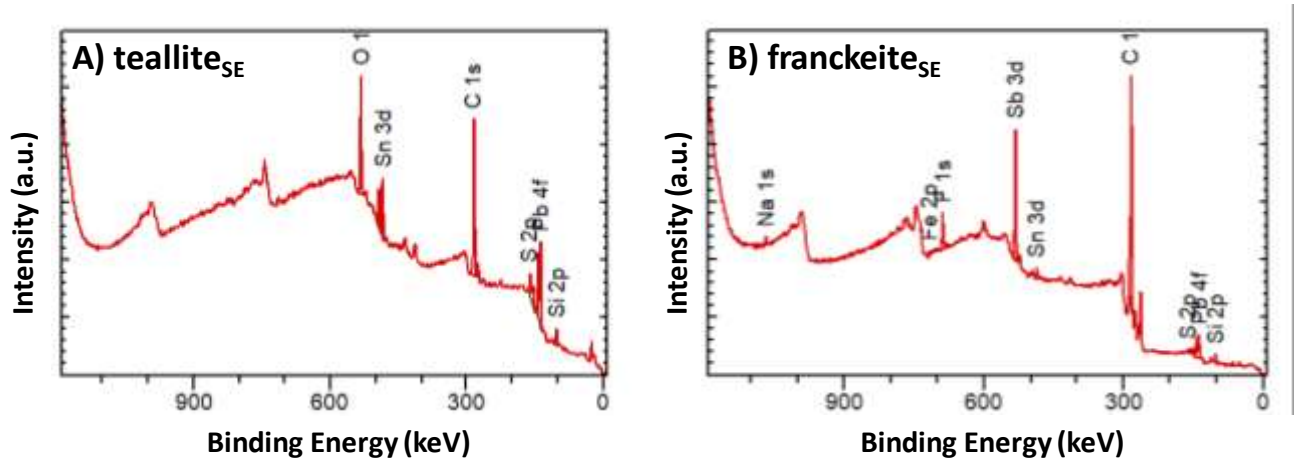

Figure S8. XPS wide survey spectra of the shear-exfoliated sulfosalts: (A) teallite$_{SE}$ and (B) franckeite$_{SE}$, referenced to the carbon C 1s peak at 284.5 eV.

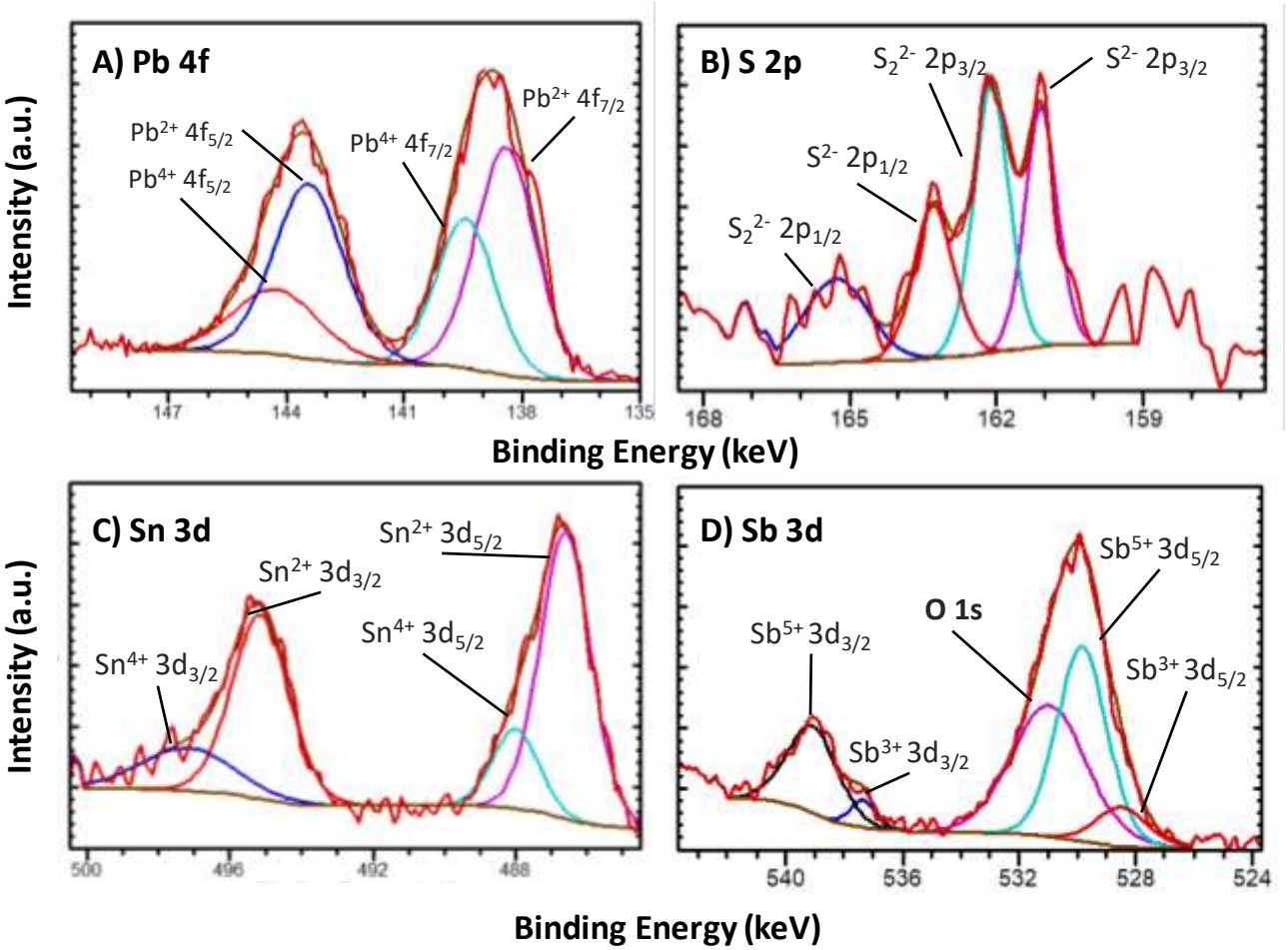

Figure S9. High-resolution spectra and deconvolution of peaks for franckeite$_{SE}$.

Table S3. Quantification of individual elements of bulk and shear exfoliated sulfosalts obtained from the XPS survey spectra.

		Sample / % conc.			
	Position	**Franckeite$_{bulk}$**	**Franckeite$_{SE}$**	**Teallite$_{bulk}$**	**Teallite$_{SE}$**
Si 2p	101.5	4.9	4.2	2.5	7.3
Pb 4f	138.5	8.6	1.7	4.9	4.2
S 2p	161.5	17.6	3.6	17.7	13.9
C 1s	284.5	62.1	82.1	43.7	53.5
Sn 3d	486.5	1.6	0.3	7.8	3.7
Sb 3d*	531.5	3.8	2.5	—	—
O 1s	532.4	—	—	23.5	16.7
F 1s	688.5	1.4	4.4	—	—
Fe 2p	716.5	—	0.4	—	—
Na 1s	1068.5	—	0.7	—	—

* for franckeite there is overlapping of Sb 3d and O 1s signal

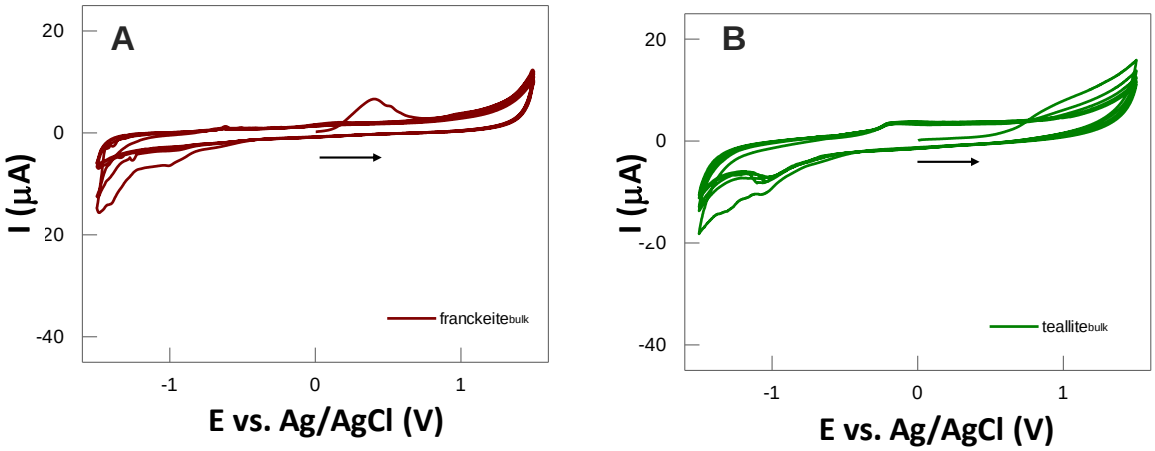

Figure S10. CVs of inherent electrochemistry for bulk crystals franckeite (A) and teallite (B). Conditions: phosphate-buffer (PBS, 0.1 M, pH 7.2), 5 cycles, 100 mV s^{-1}.

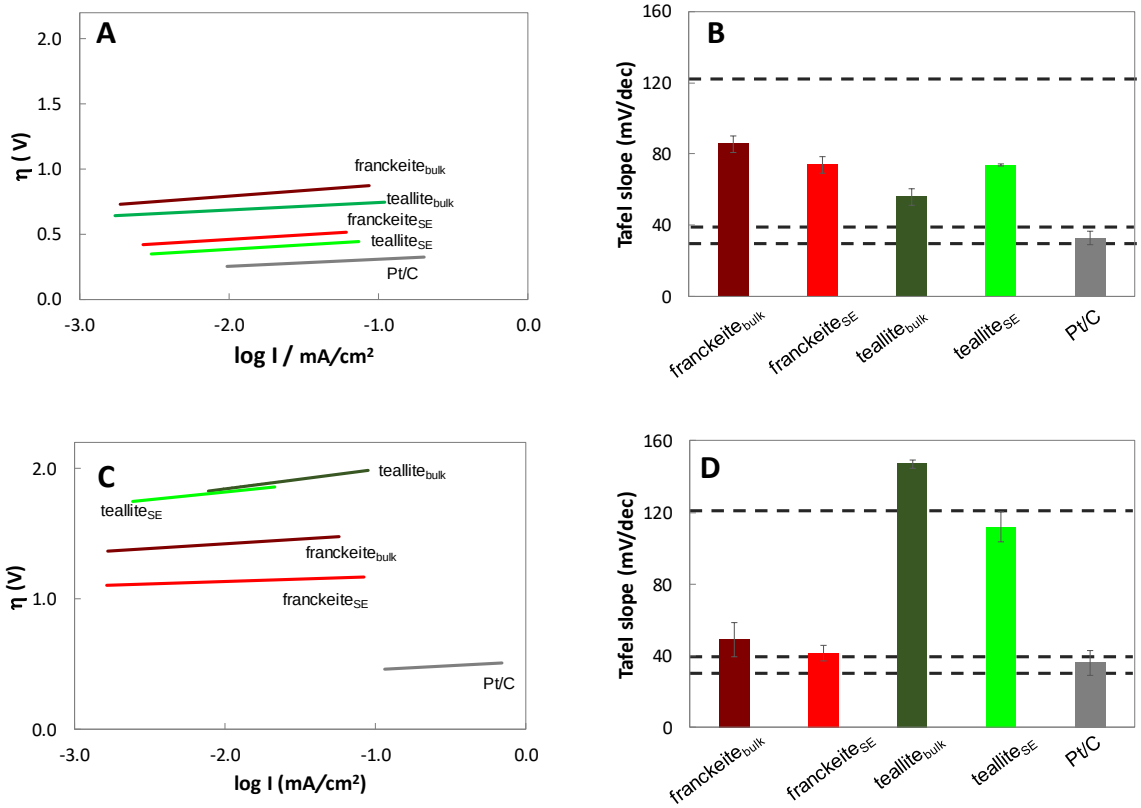

Figure S11. Tafel plot for the HER in acidic (A) and alkaline (C) derived from LSV polarization curves. Tabulated values for the Tafel slope; dotted lines at 120, 40 and 30 mV/dec correspond to the Volmer, Heyrovský and Tafel mechanisms, respectively. Error bars correspond to standard deviations based on triplicate measurements (B and D).

Supplementary Note 1 – Franckeite crystal structure

Captions of the minerals and exfoliation process are shown in **Figure S1**. Franckeite ($Pb_5Sn_2FeSb_2S_{14}$) has thin tabular crystals, usually massive, radiating or foliated with a triclinic symmetry.[1,2] Franckeite is composed of alternating sequences of weakly bound, multi-stacked PbS and SnS_2 layers separated by van der Waals gaps (Scheme 1).[1,2] The strong compositional segregation for Pb and Sn atoms leads to markedly different electronic band structures for the different layers, whose overall properties may be intricate due to Pb/Sb and Sn/Fe partial substitutions.[3–5] These type of misfit or incommensurate in-plane layered structures have two layers of different periodicity in their crystal structure.[6,7] Each pseudotetragonal (Q-layer) is a Pb-rich layer with four atoms layer thick, consisting of two MS sheets (M= Pb^{2+}, Sn^{2+} and Sb^{3+}) and the Pb atoms in each PbS sheet forms distorted square-pyramids with the surrounding S atoms (Scheme 1). The pseudohexagonal (H-layer) is an MS_2 type layer, in which Sn^{4+} or Fe^{2+} atoms are intercalated between two sheets of S atoms, and each M atom forms an MS trigonal prism.

Supplementary Note 2 - Shear exfoliation procedure

A pre-exfoliation step to clean the minerals was therefore introduced for removal of oxides and impurities. Typically, 500 mg of starting materials were initially grinded, followed by sonication in 5 mg/mL aqueous surfactant sodium cholate (SC) for 10 minutes in an ice bath sonicator (FB11203, 80KHz, pulse mode). Suspensions were then centrifuged with a Beckman Coulter Allegra 64R centrifuge for 1 hour at 4 Krpm with the supernatant being decanted and discarded with the sediment being retained. The crystals were then recovered by filtration.

The pre-treated sulfosalts were then submitted to shear dispersion and exfoliation in fresh aqueous surfactant SC for 1 h mixing using an immersion 750 W hand blender at full speed. The blender foot consists of stainless-steel with 4 blades, from Bosch (MSM 67190GB), as shown in Figure S1. To avoid degradation of plastic components and overheating of the rotors appliances, 2 min on/1 min off cycles were followed. To prevent potential degradation of the samples or boiling the solvent ice baths were used (**Figure S1**).

After shear exfoliation, the suspensions were centrifuged using Beckman Coulter Allegra 64R centrifuge at 1 Krpm for 1 hour. The top 75% of the dispersions were decanted and the bottom 25% was not processed, as it contains poorly or non-exfoliated material. Water was added to the dispersion and the following centriguation was done at 3 Krpm for 1 hour. In this case, only the bottom 40% was proced. For further removal of aqueous surfactant, aqueous washing by 3 successive centrifugations at 10 Krpm for 0.5 h were employed.

The bottom 20 % of the resulting suspensions was separated, which contains the shear-exfoliated materials. These were then vacuum dried at 60 °C for characterization and electrochemical performance studies. Starting materials shall be referred to as $sulfosalt_{bulk}$ and exfoliated materials as $sulfosalt_{SE}$. A visual representation of the centrifugations steps is shown in **Scheme S1, bottom**.

Supplementary Note 3 - Considerations on the shear exfoliation process

Solution-based techniques for preparation of 2D layered nanosheets can be divided into wet chemical synthesis methods (bottom-up) and liquid-phase exfoliation methods (top-down). The liquid-phase exfoliation is described as a dispersion/exfoliation method, and the concept is to weaken the interaction of adjacent layers of layered materials, thus decreasing the number of layers. To achieve this goal, dispersion chemicals, are necessary, which greatly determine the exfoliation yield and quality of exfoliated materials.

High-shear mixing has been shown to be an effective approach for the exfoliation of large quantities of 2D layered materials, providing a viable path for the industrial scaling of applications based on these layered materials.[8] Other powerful liquid phase methods such as sonication can damage 2D flakes with high induction of defects. Shear force exfoliation can be considered as a *soft* method, which is a less energy-intensive shearing process to exfoliate layered materials in organic solvents or, preferably in aqueous media.

Shear force exfoliation process. Natural occurring layered materials have uncontrolled impurities which can disturb the stability of suspensions and influence electrochemical properties. In the chosen media, the minerals are submitted to a residual exfoliation process (≤ 10% of the total time). The resulting suspension is then centrifuged to remove superficial oxides and impurities. Deposited crystals are then dispersed in a freshly prepare surfactant solution and exfoliation process can proceed.

In the current work, shear mixing an immersion 750 W hand blender, all stainless-steel foot with 4 blades was used (**Figure S1**). The immersion blender operates predominately in laminar regime at the main body of the mix, with constant shear forces that promote the delamination of layers from crystal materials (**Scheme S1 top**). Hand blender position can be adjusted to maximize fluid circulation and minimization of foam along the process.
As proposed by Paton et al.[9] for lab-scale shear mixer, initial high-speed rotation of the immersion blender rotor blades within mixing work-head employs a powerful suction, drawing solvent and minerals upwards from the bottom of the vessel and into the blades (Scheme S1, top left side). Crystals are then subjected to collisions (Scheme S1, top right) and delamination in between the blades and the inner wall of the work-head. This is followed by intense hydraulic shear as the materials are expelled outwards through the cavities of the work-head and circulated into the main body of the mix (Scheme S1, top right). Within the bulk of the mix, driven by centrifugal force, materials circulates at high rpm in a predominately-laminar regime. A continuous feed of material is drawn into the blades, looping the mixing cycle. The effect of the radial expulsion, laminar flow and suction into the blade is to set up a circulation pattern that minimizes solution aeration. A series of collisions of the crystals with the blades, edges, boarders and random collisions between fragmented sheets promotes lateral downsizing. The shear force, affinity of the surfactant for layered materials and their lateral self-lubricating ability, makes this exfoliation process less harsh and guarantees high quality nanosheets.

Household kitchen blenders. Commercial immersion hand blenders can be considered as a low-cost version of a lab/industrial scale of a rotor stator mixer. We consider important that the foot of the blender is fully *inox* steel, avoiding any polymeric components, making it therefore a versatile choice for all different media.

Temperature. Several authors[8] and ourselves also find that it is crucial to control the temperature during the blending operation. Thus, the goblet of the hand blender mixer was kept in an ice bath during off cycles (Figure S1). Working in overheated media causes degradation of blender components, results in lower dispersed concentration and can cause chemical degradation of the exfoliated nanosheets.

Isolation of Exfoliated Nanosheets. Afterwards to shear exfoliation, the suspensions were centrifuged and the top 75% were separated for aqueous surfactant removal, by aqueous washing and secondary centrifugations at high rotation speeds (Scheme S1, bottom). Depending on the density of the material and medium, total centrifugation time will require adjustments. Initial centrifugation at low-speed centrifugations allows to remove thicker and poorly exfoliated material. Subsequently the short, high-speed centrifugations allows for the isolation of exfoliated material and removing excess of surfactant. Complete removal of the surfactant might not be possible as surfactant can be adsorbed by nanosheets. Nevertheless, XPS wide scan of the exfoliated materials can be a helpful tool to control the amount of Na, as an indicative of the surfactant residue.

Yields. Different empirical equations have been proposed for shear force exfoliation production[9]. Big volumes mean less probability of collision between crystals, impacts with the blades and less energy efficiency. Thus, we suggest the working volume to be a few mL above of what is enough to leave the blades fully immersed when working with these kind of kitchen blenders.
Intuitively, the higher concentration of starting materials, the higher quantity of exfoliated nanomaterial is expected. This is true up to the point where dispersed concentration of the media saturates.[8] Nonetheless, 1 g/L is the concentration commonly used by researchers. Working with high power blenders at full speed maximizes yield, but overheating of appliances is a setback that slows the process with unavoidable on/off cycles. Longer processing times can lead to higher yields, but it is not yet clear the moment when degradation is induced to the quality of the materials.
Typically, 2−6 g/L aqueous surfactant SC is recommended (herein 5 g/L). The role of surfactant concentration is currently lacking; however, it has been found that nanosheet size and thickness varies with the surfactant concentration

used.[8] When using surfactants in kitchen blenders the liquid turns a different shades of gray color as the material starts to disperse, but undesirably bubbles begin to form as shown in Figure S1. Using immersion hand blender, allows to minimize the foam permanence and more material can be exfoliated.
The final yield of the exfoliation processes is not always mention. In the present case, the yield obtained is comparable to shear exfoliation of BP, TMDs, etc. (≤ 10%), even when comparing the results with longer processing times and toxic organic media. To the best of knowledge, previous reports on the exfoliation of franckeite and teallite have used mechanical peeling or liquid phase exfoliation by sonication, using different organic media (MNP, IPA, etc.).[10–14] There are no direct mentions of the obtained yields.

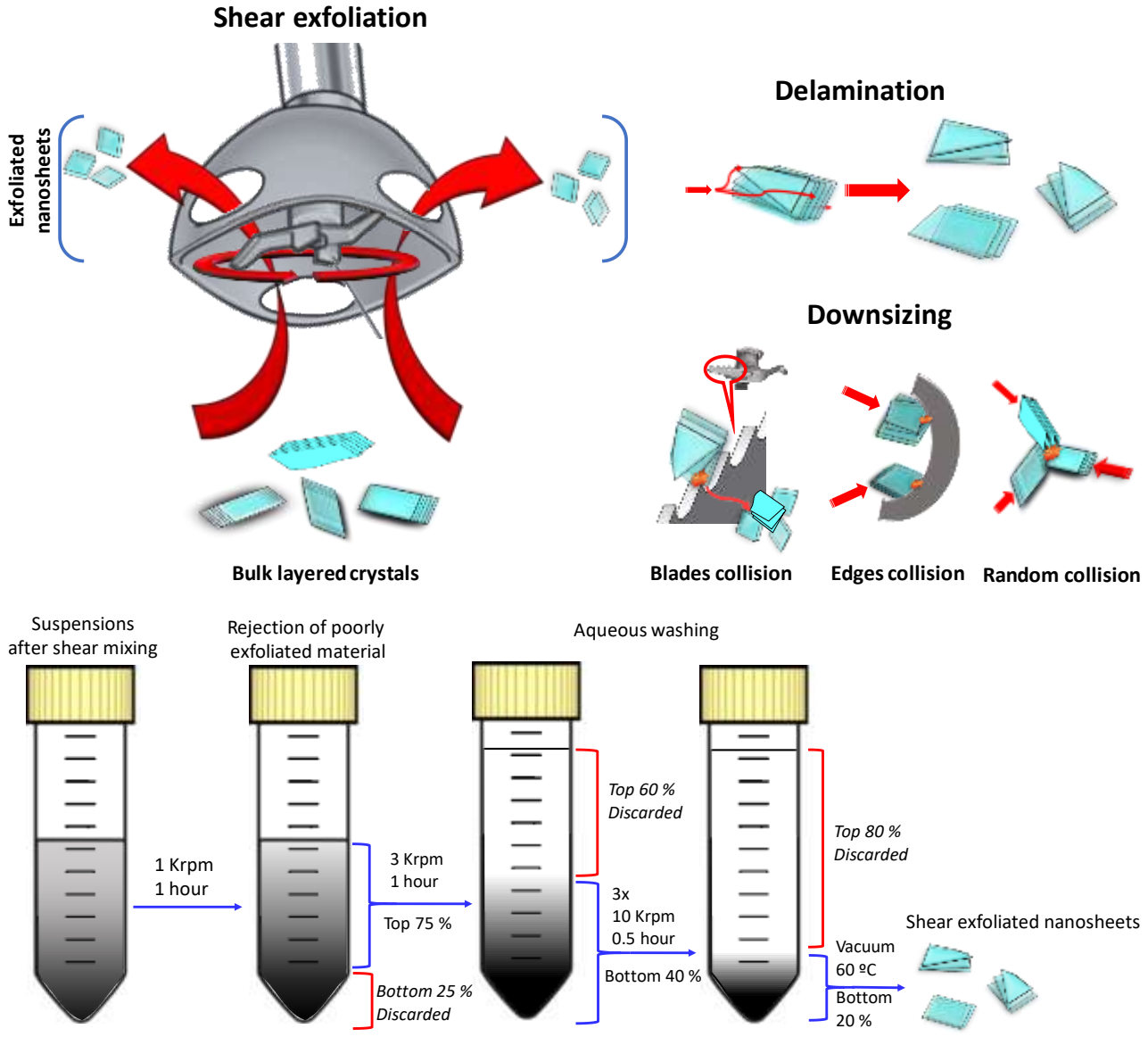

Scheme S1. Top: Simplified illustration of the shear exfoliation processes by delamination and downsizing mechanisms of bulk crystal. Bottom: Schematic showing isolation of shear exfoliation nanosheets centrifugation with the rpm iterations used in this work.

Supplementary Note 4 - HER Mechanism

The HER mechanism has been thoroughly studied, and there are two widely accepted mechanisms. Both are two-step mechanisms that begin with the adsorption of a proton onto the electrode surface through an electrochemical reduction process (Volmer step):
Volmer adsorption step:

$$H_3O^+ + e^- \rightarrow H^\bullet_{ads} + H_2O \qquad b \approx 120mV/dec \quad (1)$$

This step is followed either by the recombination of two hydrogen atoms adsorbed on the surface (Tafel desorption step):

$$H^\bullet_{ads} + H^\bullet_{ads} \rightarrow \uparrow H_2 \qquad b \approx 30mV/dec \quad (2)$$

or by the direct bonding of a hydrated proton with the adsorbed hydrogen atom which includes an electron transfer from the electrode surface (Heyrovsky step).

$$H_{ads} + H_3O^+ + e^- \rightarrow \uparrow H_2 + H_2O \quad b \approx 40mV/dec \quad (3)$$

It is important to highlight the fact that HER is a two-step reaction involving adsorption of hydrogen ion and desorption of hydrogen molecule. Depending on the electrode surface, either the first or the second step can be rate determining.

References

1 E. Makovicky, V. Petricek, M. Dusek and D. Topa, *Am. Mineral.*, 2011, **96**, 1686–1702.
2 S. Wang and K. H. Kuo, *Acta Crystallogr. Sect. A Found. Crystallogr.*, 1991, **47**, 381–392.
3 T. B. Williams and B. G. Hyde, *Phys. Chem. Miner.*, 1988, **15**, 521–544.
4 G. H. Moh, *Mineral. Petrol.*, 1987, **36**, 191–204.
5 H. Bengel, S. Jobic, Y. Moëlo, A. Lafond, J. Rouxel, D. K. Seo and M. H. Whangbo, *J. Solid State Chem.*, 2000, **149**, 370–377.
6 A. Meerschaut, *Curr. Opin. Solid State Mater. Sci.*, 1996, **1**, 250–259.
7 C. K. Chua, Z. Sofer, O. Jankovský and M. Pumera, *ChemPhysChem*, 2015, **16**, 769–774.
8 C. Backes, T. M. Higgins, A. Kelly, C. Boland, A. Harvey, D. Hanlon and J. N. Coleman, *Chem. Mater.*, 2017, **29**, 243–255.
9 K. R. Paton, E. Varrla, C. Backes, R. J. Smith, U. Khan, A. O'Neill, C. Boland, M. Lotya, O. M. Istrate, P. King, T. Higgins, S. Barwich, P. May, P. Puczkarski, I. Ahmed, M. Moebius, H. Pettersson, E. Long, J. Coelho, S. E. O'Brien, E. K. McGuire, B. M. Sanchez, G. S. Duesberg, N. McEvoy, T. J. Pennycook, C. Downing, A. Crossley, V. Nicolosi and J. N. Coleman, *Nat. Mater.*, 2014, **13**, 624–630.
10 E. Burzurí, M. Vera-Hidalgo, E. Giovanelli, J. Villalva, A. Castellanos-Gomez and E. M. Pérez, *Nanoscale*, 2018, **10**, 7966–7970.
11 A. J. Molina-Mendoza, E. Giovanelli, W. S. Paz, M. A. Niño, J. O. Island, C. Evangeli, L. Aballe, M. Foerster, H. S. J. van der Zant, G. Rubio-Bollinger, N. Agraït, J. J. Palacios, E. M. Pérez and A. Castellanos-Gomez, *Nat. Commun.*, 2017, **8**, 14409.
12 M. Velický, P. S. Toth, A. M. Rakowski, A. P. Rooney, A. Kozikov, C. R. Woods, A. Mishchenko, L. Fumagalli, J. Yin, V. Zólyomi, T. Georgiou, S. J. Haigh, K. S. Novoselov and R. A. W. Dryfe, *Nat. Commun.*, 2017, **8**, 14410.
13 K. Ray, A. E. Yore, T. Mou, S. Jha, K. K. H. Smithe, B. Wang, E. Pop and A. K. M. Newaz, *ACS Nano*, 2017, **11**, 6024–6030.
14 A. Łapińska, A. Taube, M. Wąsik, G. Z. Żukowska, A. Duzynska, J. Judek and M. Zdrojek, *J. Raman Spectrosc.*, 2017, **48**, 479–484.